Heat Mass Transfer (2009) 45:427–441
DOI 10.1007/s00231-008-0435-z

ORIGINAL

# Energy storage in fluid saturated porous media subjected to oscillatory flow

**Chanpreet Singh · R. G. Tathgir · K. Muralidhar**

Received: 22 January 2008 / Accepted: 28 August 2008 / Published online: 23 September 2008


**Abstract** Transient thermal effects in a porous medium subjected to oscillatory flow of hot and cold fluid are studied. The governing equations of thermal non-equilibrium model have been numerically solved by a finite difference scheme. The amplitude of temperature fluctuation, a parameter relating to the energy storage, is seen to vary significantly with distance and time. The storage of energy is largely governed by fluid to solid phase thermal storage capacity ratio. Effects arising from changes in bed parameters are discussed.

## List of symbols

| | |
|---|---|
| $A_{IF}$ | specific area of the porous insert ($m^{-1}$) |
| $A_f$ | non-dimensional value of $A_{IF}$: $A_{IF\times}R$ |
| $Bi$ | Biot number (h $R(k_s)^{-1}$) |
| $C_p$ | specific heat (J(kg K)$^{-1}$) |
| $d_p$ | particle diameter (m) |
| $E$ | energy (J) |
| $h_{sf}$ | heat transfer coefficient at the particle surface ($Wm^{-2}$ $K^{-1}$) |
| $K$ | thermal conductivity (W (m K)$^{-1}$) |
| $K$ | weighted ratio of thermal storage capacities of the fluid and solid phase, $\frac{(1-\varepsilon)(\rho c_p)_s}{(\varepsilon)(\rho c_p)_f} = \frac{1-\varepsilon}{\varepsilon\beta}$ |
| $(k_{eff,f})_r$ | effective thermal conductivity of the fluid in $r$-direction (W (m K)$^{-1}$) |
| $(k_{eff,f})_z/k_f$ | dispersion coefficient of fluid in $z$-direction |
| $L$ | length of porous domain scaled by R |
| $N$ | cycle number |
| $Nu$ | Nusselt number, hR/k |
| $Pe$ | Peclet number, $Re \times Pr$ |
| $Q$ | interphase heat transfer |
| $Pr$ | Prandtl number ($\mu C_p/k$) |
| $R$ | non-dimensional radial coordinate |
| $Re$ | Reynolds number ($\rho UR/\mu$) |
| REV | representative elementary volume |
| $T$ | time, non-dimensionalized by $\alpha_f/R^2$ |
| $t_p$ | time period of oscillations (s) |
| $R$ | characteristic length scale, m also the pipe radius |
| $T$ | non-dimensional temperature: $(T- T_C)/\Delta T$ |
| $\Delta T$ | reference temperature difference ($T_H - T_C$) |
| $U$ | non-dimensional axial velocity scaled with $U$ |
| $U$ | characteristic fluid velocity equal to the average velocity in the tube ($ms^{-1}$) |

## Greek symbols

| | |
|---|---|
| $\alpha$ | thermal diffusivity ($m^2$ $s^{-1}$) |
| $\beta$ | thermal capacity ratio between the fluid and the solid phases |
| $\varepsilon$ | porosity of the medium |
| $\lambda$ | thermal conductivity ratio between the fluid and the solid phases |
| $\mu$ | dynamic viscosity of the fluid (kg (m s)$^{-1}$) |
| $\nu$ | kinematic viscosity of the fluid ($m^2$ $s^{-1}$) |

C. Singh (✉)
Mechanical Engineering Department,
University College of Engineering, Punjabi University,
Patiala 147002, India
e-mail: singh.chanpreet@rediffmail.com

R. G. Tathgir
Lala Lajpat Rai Institute of Engineering and Technology,
Moga 142001, India

K. Muralidhar
Department of Mechanical Engineering,
Indian Institute of Technology Kanpur, Kanpur 208016, India

$\rho$ material density (kg $m^{-3}$)
$\omega$ frequency of oscillations, $2\pi/t_p$ (rad/s)
$\omega t$ phase angle (radians)

**Subscripts**

A ambient conditions
C cold water temperature (K)
D particle diameter
F fluid phase
H hot water temperature (K)
M porous medium
ND non-dimensional quantity
S solid phase
P time-period

## 1 Introduction

Energy storage using a porous medium is an attractive method of storing thermal energy and reusing it at a later point of time. This effect can be obtained by using fixed porous solid mass such as closely packed mesh screens or spherical beads through which hot and cold fluids flow alternately [1, 2]. The energy is stored in the solid phase when hot fluid flows through the pores and is released to the cold fluid. The periodic flow of fluid through opposite ends of the porous bed creates an oscillatory flow condition that has wide applications in waste-heat recovery units of gas turbines and enhancement of cooling of electronic equipments [3]. A specific example is a regenerator used in a Stirling cycle. Here, the porous medium acts as a thermal sponge, absorbing energy in its solid phase when exposed to the hot fluid and releasing it to the cold fluid at a later stage of the cycle. As energy exchange takes place from and to the solid phase, temperature differentials are set up within the representative elementary volume. The estimation of temperature differential between the two phases is important for the performance of the storage system. This is called thermal non-equilibrium, Amiri and Vafai [4]. Mathematical modeling should consider separate temperatures for the two phases within the representative elementary volume with interphase heat transfer connecting them [4, 5].

Various investigations study thermal effects related to energy storage systems and oscillatory flow in porous media. In an earlier work, Koh and Colony [6] and Koh and Stevens [7] showed the use of porous media for cooling high temperature surfaces. In the work related to energy storage, Bejan [8] stated that a second law technique should be used for analysis of the storage system to improve thermodynamic availability of the stored energy. Beasley and Clark [9] investigated the transient response of a packed bed for energy storage using experimental and numerical techniques. Muralidhar and Suzuki [10] proposed two models for flow and heat transfer in Stirling cycle regenerators. The first considers flow and heat transfer at the scale of a wire that constitutes the mesh and second is a complete non-Darcy, thermal non-equilibrium model for the mesh treated as a porous medium. Chikh et al. [11] studied numerically the heat transfer enhancement between two parallel plates using intermittently placed porous blocks. Peak et al. [12] studied experimentally the cool-down characteristics of a porous medium in a uniform pulsating flow while adding an oscillatory component to the mean flow. The cooling effectiveness was seen to increase as the amplitude of pulsations and the frequency were increased. Muralidhar and Suzuki [13] analyzed oscillatory flow and heat transfer in a regenerator using the thermal non-equilibrium model treating the mesh screen as porous inserts. A short length of regenerator resulted into a lower effectiveness but a longer length led to underutilized regenerator space. Dincer and Rosen [14] showed that, with the use of a suitable storage system, the running cost of the plant reduces by as much as 50%, thereby lowering the peak hour demand of electricity. Fu et al. [15] experimentally studied wall heat transfer in a porous channel subjected to oscillating air flow. The surface temperature distribution for oscillating flow was found to be more uniform than that for steady flow. The length averaged Nusselt number in oscillatory flow was also higher. The reason was attributed to an increased effective thermal conductivity in the presence of the porous region. Porous medium subjected to oscillatory flow can act as a good heat sink and as an effective method of rapid heat dissipation, Leong and Jin [16]. Byun et al. [17] studied analytically the thermal behavior of porous medium under oscillating flow conditions. The temperature oscillations in solid and fluid phase were seen to vary with thermal properties, ratio of thermal storage capacities of solid and fluid phases, interphase heat transfer of the porous medium. Cheralathan et al. [18] used numerical and experimental techniques to study the effect of porosity and inlet fluid temperature variation on the performance of a cool energy storage system.

Energy storage properties of a porous bed under oscillatory flow conditions are obtained in this study using a thermal non-equilibrium model. These properties depend on those of the solid and the fluid phases; other properties of interest are the frequency of oscillation, its amplitude, particle size, and overall linear dimensions. To generate a variety of property ratios, the solid phase has been taken be spherical particles of glass and mild steel, while the flowing medium is water. The effectiveness of the porous bed for energy storage is calculated as the fraction of incoming thermal energy that is contained in the bed at the end of a half-cycle. Temperature profiles govern the performance of

the storage system and are presented at various instants of time within a cycle.

## 2 Mathematical model

Figure 1 shows a representation of an energy storage system. Figure 1a shows the physical model; the beads are closely packed inside a tube of radius $R$. The length of the tube in non-dimensional form is $L$. The porous bed is assumed to be water-saturated and maintained initially at zero temperature everywhere, i.e., the cold-water temperature. The fluid velocity is a sinusoidal function of time. Hence, it changes direction every half-cycle. Typical temperature profiles in the fluid phase are shown in Fig. 1b. Here, the $x$-axis is distance from the respective ends, i.e., the distance from hot end during the hot phase and from cold end during the cold phase, and the $y$-axis is dimensionless temperature.

During the hot phase, hot fluid enters the bed through one of the ends and the temperature of the bed increases. The rise is higher near the hot end and a temperature profile with respect to distance develops as in Fig. 1b. The temperature is unity, the maximum value, at $z = 0$ but its value at $z = L$ should be close to zero. It ensures that energy leaving the bed through the cold end is small. In the cold phase, the cold water enters the domain through the opposite end and the temperature of the bed diminishes. The temperature profile during the cold phase is shown by a line sloping up, Fig. 1b. The temperature is zero at the cold end but should be close to unity at the hot end for maximum utilization of stored energy. During the hot phase, the temperature at a location rises due to storage of energy but falls during the cold phase due to retrieval. Hence a cyclic change in temperature occurs at every location in the bed. During the unsteady period, the profiles change from one cycle to another but when the cyclic steady state is reached, no change occurs at corresponding instants of two successive cycles.

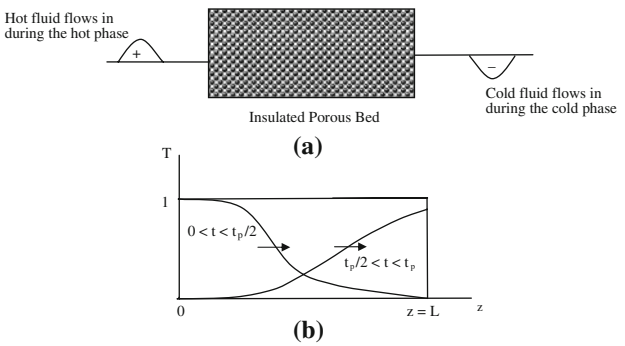


**Fig. 1** The schematic representation of an energy storage system. **a** Physical model, **b** expected temperature profiles

The governing equations are obtained from a thermal non-equilibrium model of heat transfer in the porous medium [4, 13]. In this approach, individual temperatures are assigned to the two phases and inter-phase heat transfer is permitted between them. The model is thus capable of unequal temperatures between the solid matrix and the flowing fluid. The governing equations adapted from [4, 13, 20, 24] are presented below in the non-dimensional form.

### 2.1 Equation model

$$\text{Fluid}: \varepsilon\left(\frac{1}{Pe}\frac{\partial T}{\partial t}+\frac{u}{\varepsilon}\frac{\partial T}{\partial z}\right) = \frac{1}{Pe}\left(\frac{\partial}{\partial z}\left(\left[\frac{(k_{eff,f})_z}{k_f}\right]\frac{\partial T}{\partial z}\right)+\frac{1}{r}\frac{\partial}{\partial r}\left(\left[\frac{(k_{eff,f})_r}{k_f}\right]r\frac{\partial T}{\partial r}\right)\right) - \frac{NuA_f}{Pe}(T_f - T_s) \tag{1}$$

$$\text{Solid}: \frac{(1-\varepsilon)}{Pe}\frac{\partial T}{\partial t} = \frac{\beta/\lambda}{Pe}\left(\frac{\partial}{\partial z}\left(\left[\frac{k_{eff,s}}{k_s}\right]\frac{\partial T}{\partial z}\right)+\frac{1}{r}\frac{\partial}{\partial r}\left(\left[\frac{k_{eff,s}}{k_s}\right]r\frac{\partial}{\partial r}\right)\right) + \frac{NuA_f\beta}{Pe}(T_f - T_s) \tag{2}$$

In Eq. 1, the term to the left of the equality sign is advection, the first term to the right is diffusion while the last term $\frac{NuA_f}{Pe}(T_f - T_s)$ refers to the heat transfer from the fluid to solid phase. The symbol $A_{IF}$ is the interfacial area between the fluid and the solid phases per unit volume of the porous medium. Symbol $T$ represents the dimensionless temperature given by $(T - T_C)/(T_H - T_C)$, a value between zero and unity. It is the fluid phase temperature in Eq. 1 and the solid phase temperature in Eq. 2. The length scale is the tube radius $R$ and the time scale is $R^2/\alpha$. The velocity $u$ appearing in the equations is the Darcian velocity, namely the velocity obtained by locally averaging the energy equation over a small volume of the porous medium. The thermal conductivities in the 2-equation model are corrected for dispersion effects as follows [21, 22]:

$$\text{Longitudinal}: k_{eff,fz} = \varepsilon k_f + 0.5Pek_f \tag{3}$$

$$\text{Transverse}: k_{eff,fr} = \varepsilon k_f + 0.1Pek_f \tag{4}$$

The following expression has been used for Nusselt number that represents solid-to-fluid heat transfer [21, 22]:

$$Nu_p = 2 + 1.1Pr^{0.33}Re_p^{0.6} \tag{5}$$

In the above equation, the non-dimensional numbers $Nu_p$ and $Re_p$ are defined based on the particle diameter $d_p$.

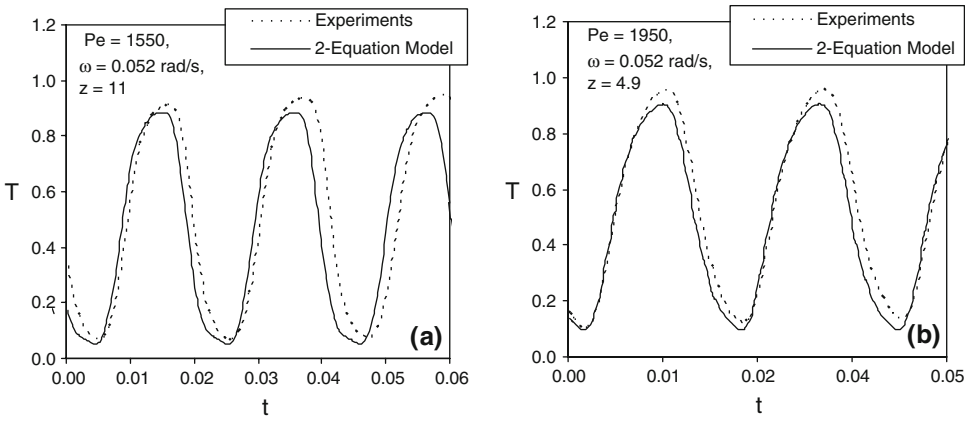


**Fig. 2** The validation of 2-equation model with experimental results for frequency response of the porous bed. **a** Glass-water bed, **b** steel-water bed

In Eqs. 1 and 2, these quantities are expressed in terms of the tube radius. The specific surface area of the porous bed composed of spheres is given as [19]:

$$A_f = \frac{6(1-\varepsilon)R}{d_p} \tag{6}$$

The governing equations subjected to suitable initial and boundary conditions have been numerically solved by an implicit finite difference method. The QUICK approach [23] is used to approximate the first order convective terms, while central differencing scheme is used for the second order partial derivatives in space. A forward difference formula evaluates the time derivatives. Gauss-Seidel iterations are used to solve the system of algebraic equations. Time steps and space grids are chosen such that the results obtained are independent of the number of time steps and nodes. Typically, the time step is 0.01% of the total time and grid size is 0.1% of the total length of the porous region. The number of cycles is chosen large enough so that cyclic steady state is reached. The numerical algorithm used is quite similar to the one described in [13]. It has been further validated against experimental results as shown in Fig. 2 for glass- and steel-water beds [24] at a frequency of 0.052 rad/s.

## 3 Initial and boundary conditions

Additional conditions of flow and temperature are incorporated in the numerical simulation through appropriate boundary conditions. The velocity is sinusoidal, being positive during the hot phase and negative during the cold phase, i.e.,

$$u = u\,\sin(\omega t) \text{ with Hot phase : } 0^\circ < \omega t < 180^\circ; \quad \text{Cold phase : } 180^\circ < \omega t < 360^\circ \tag{7}$$

In the hot phase, hot fluid flows in through the hot end and the fluid temperature is assigned a unit value. The outflow boundary condition is of the gradient type, namely the temperature derivative is zero in the axial direction for both the phases at $z = L$. Hence

$$T_{z=0} = 1 \quad \text{and} \quad \left(\frac{\partial T}{\partial z}\right)_{z=L} = 0 \tag{8}$$

In the cold phase, the flow direction is reversed and the cold fluid enters through the opposite cold end. Here the temperature is assigned a value of zero. The fluid and the solid phase temperatures are assigned zero gradients in the axial direction at $z = 0$. Hence

$$T_{z=L} = 0 \quad \text{and} \quad \left(\frac{\partial T}{\partial z}\right)_{z=0} = 0 \tag{9}$$

Along the tube axis, symmetry of the temperature field is assumed for both the fluid and the solid phases:

$$\left(\frac{\partial T}{\partial r}\right)_{r=0} = 0 \tag{10}$$

The heat flux is prescribed for heat loss through the tube wall for the fluid and the solid phase in terms of Biot number as follows

$$-\left(\frac{\partial T_f}{\partial r}\right)_{r=1} = \frac{Bi}{\lambda}\left((T_f)_{r=1} - T_a\right) \quad \text{and} \quad -\left(\frac{\partial T_s}{\partial r}\right)_{r=1} = Bi\left((T_s)_{r=1} - T_a\right) \tag{11}$$

## 4 Effectiveness of energy storage

As the hot fluid enters the bed, the energy is stored in the solid as well as the fluid phases contained in the bed and temperature of the bed rises. For a perfectly insulated bed, the stored energy is calculated by the difference of incoming and outgoing fluid energies. During the initial unsteady period, the stored and the retrieved energies are unequal. Once the cyclic steady state is reached, these two are equal.

The stored energy during a hot phase given as

$$E_{stored} = \int_0^{t_P/2} (E_{in} - E_{out})dt \tag{12}$$

Similarly, the energy retrieved during the cold phase is given as

$$E_{retrieved} = \int_{t_P/2}^{t_P} (E_{out} - E_{in})dt \tag{13}$$

The stored energy is given as

$$E_{stored} = (\rho c_P)_f u \frac{2}{\omega} \pi R^2 (T_H - T_C)_{z=0} - (\rho c_P)_f \pi R^2 \int_0^{t_P/2} u \sin(\omega t)(T - T_C)_{z=L} dt \tag{14}$$

The cold fluid enters the bed at a temperature of $T_C$ and its energy is zero. It leaves the hot end with a temperature of $T$. Simplifying Eq. 14, we get

$$E_{retrieved} = \int_{t_P/2}^{t_P} (\rho c_P)_f u \sin(\omega t) \pi R^2 (T - T_C)_{z=0} dt \tag{15}$$

The effectiveness of porous medium for energy storage is the amount of energy retrieved in the cold phase to the amount of energy supplied during the hot phase. Both these energy calculations occur at the hot end. The effectiveness of the porous bed for energy storage is

$$Effectiveness = \frac{E_{retrieved}}{E_{in}} \tag{16}$$

Simplifying Eq. 16, we get

$$Effectiveness = \frac{\omega}{2} \int_{t_P/2}^{t_P} T_{z=0} \sin(\omega t) dt \tag{17}$$

The effectiveness depends upon the temperature variation at the hot end during the cold phase. If it becomes unity throughout the cycle, the effectiveness is 100%.

The difference between the stored and retrieved energies is obtained from Eqs. 14 and 15. Dividing it by the stored energy, a factor $\psi$ can be defined as

$$\psi = \frac{E_{stored} - E_{retrieved}}{E_{stored}} \tag{18}$$

Hence

$$\psi = 1 - \frac{\int_{t_p/2}^{t_P} T_{z=0} \sin(\omega t) dt}{\frac{2}{\omega} - \int_0^{t_P/2} T_{z=L} \sin(\omega t) dt} \tag{19}$$

In an exact calculation, the values of $\psi$ approach zero at steady state. The grid size and the time steps in the numerical simulation are chosen such that the factor $\psi$ is less than 0.001.

## 5 Results and discussion

Temperature profiles during the hot and the cold phases are presented. The amplitude of temperature fluctuations, degree of thermal non-equilibrium, and energy effectiveness are discussed. The effect of parameters such as domain length, forcing frequency, particle diameter and thermal properties of the solid phase are considered. The initial discussion is related to glass-water bed and models a situation where the solid and fluid properties are comparable.

### 5.1 Temperature profiles

Consider a porous bed of length $L = 10$ with glass beads of particle diameter $d_P$ contained in an insulated tube of radius $R$, the fluid medium being water. For definiteness, the ratio $R/d_P$ is set to be 12. Fluid velocities are taken to be spatially uniform though a function of time. Since the flow rate varies as a sine function of time, the corresponding Reynolds number based on the tube radius varies in a similar fashion. Its peak value of is set to be 100. It occurs at the middle of the hot and the cold phases, though in opposite directions. The frequency of oscillations $\omega$ in non-dimensional form is obtained by multiplying time in seconds, by a factor of $\frac{\alpha Pe}{R^2}$ and has been set to a value of unity. For a tube radius of 30 mm and normal ambient temperature of 25°C, the corresponding dimensional frequency is 0.095 rad/s. It corresponds to a time-period of 66 seconds. The fluid phase thermal diffusivity is 0.0144 $cm^2\ s^{-1}$ and the Peclet number is 621. The particle size is 2.5 mm and the length of the bed is 300 mm. The values of thermal storage capacity ratio $\beta$ and thermal conductivity ratio $\lambda$ are 2.2 and 0.55, respectively, for the glass-water bed.

At the start of numerical simulation, the bed temperature is zero and but rises with time as the hot fluid flows in during the hot phase. The temperature decreases with distance from the hot end, but at a particular location, it reaches its maximum value at the end of the phase, i.e., $\omega t = 180°$. In the cold phase, the temperature falls and reaches a minimum value at $\omega t = 360°$. The process of heating and cooling continues until cyclic steady state is reached. Here the temperatures at corresponding points of two consecutive cycles are equal. Figure 3 shows the temperature profiles for the glass-

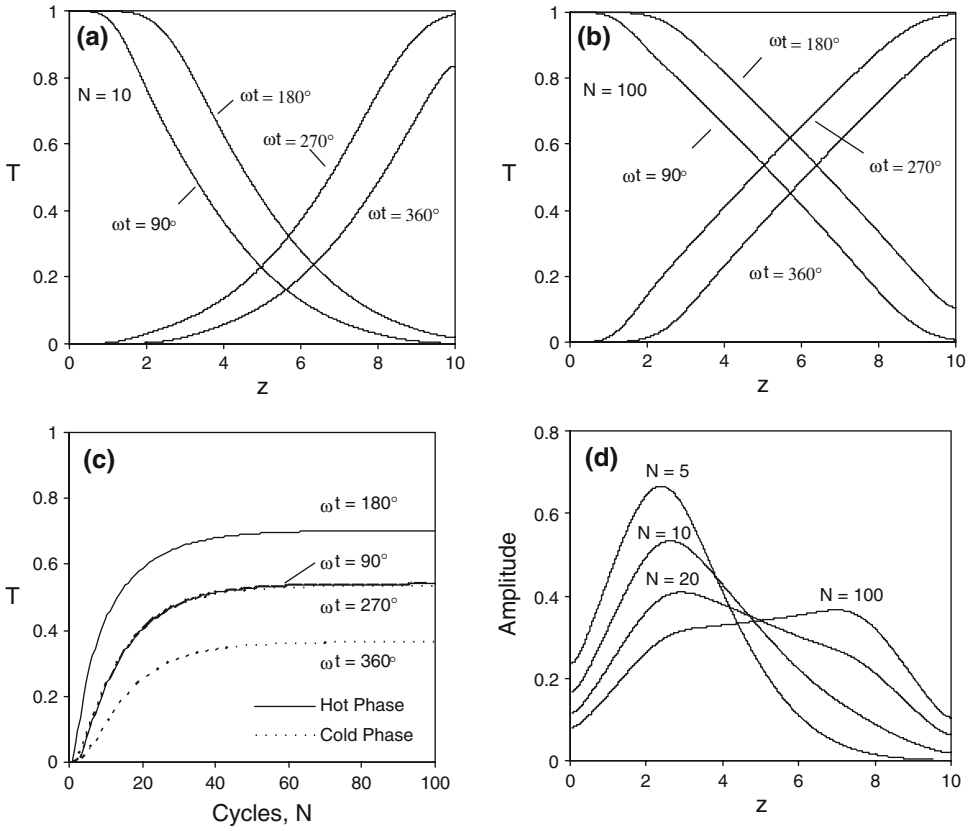


**Fig. 3** Instantaneous temperature profiles in glass-water bed. **a**, **b** The variation of fluid temperature with distance in the glass-water bed; **a** unsteady, $N = 10$; **b** steady state; **c** variation of midpoint fluid temperature with time, **d** amplitude of temperature fluctuations. $Re = 100$, $L = 10$, $\omega = 1$

water bed till cyclic steady state is reached. Figure 3a, b show the temperature profile with respect to distance from the hot and cold ends. Figure 3a shows temperature variation during the tenth cycle and Fig. 3b is for steady state. The cyclic rise of temperature at the mid-point of the bed at the end of the hot phase is shown in Fig. 3c. It is seen here that in the unsteady phase, temperature amplitudes are smaller than at steady state. Cyclic steady state is reached after around 60 cycles of pulsation. The temperatures at $\omega t = 360°$ and $\omega t = 180°$ are the lowest and the highest with values at steady state being 0.36 and 0.70, respectively. Temperature at the midpoint fluctuates between these values cyclically, yielding an amplitude (defined as the difference of the maximum and minimum temperatures) of 0.34.

Temperature fluctuations at other locations in the bed are shown in Fig. 3d. The figure can be divided into two regions about its midpoint, first in which the amplitude falls with the number of cycles and the second in which it increases. Region 1 is the portion of the bed between the hot end and the midpoint whereas the midpoint and the cold end forms region 2. The trends of amplitude are distinct for the two regions. For region 1, amplitude falls with the number of cycles but for region 2, it increases. The two regions merge at the midpoint of the bed where the amplitude is 0.34, as stated above. The amplitude variation over the length of the bed is flat in most parts except near the ends where it falls to near-zero values.

Temperature amplitudes at the hot and cold ends provide useful information. A positive value at the hot end in Fig. 3d indicates that the fluid temperature at the end of the cold phase is less than the ideal value of unity. A positive value at the cold end indicates that at the end of the hot phase, fluid temperature is greater than the ideal value of zero. These trends are also shown in Fig. 3a, b at $z = 0$ and 10. Temperature amplitudes at the hot and the cold ends approach 0.08 and 0.105 with the passage of the thermal pulses through the bed.

### 5.2 Thermal non-equilibrium

The degree of thermal non-equilibrium between the fluid and solid phases, $T_f - T_s$ during the cycle is discussed. During the hot phase, fluid temperature is higher when compared to the solid and the temperature differential is positive. It becomes negative during the cold phase when the matrix releases energy to the incoming fluid. The maximum and the minimum values of the temperature differential occur at the middle of the two phases and are numerically equal.

Figure 4 shows the variation of degree of thermal non-equilibrium between the two phases of the porous medium with respect to distance from the hot end at various cycles

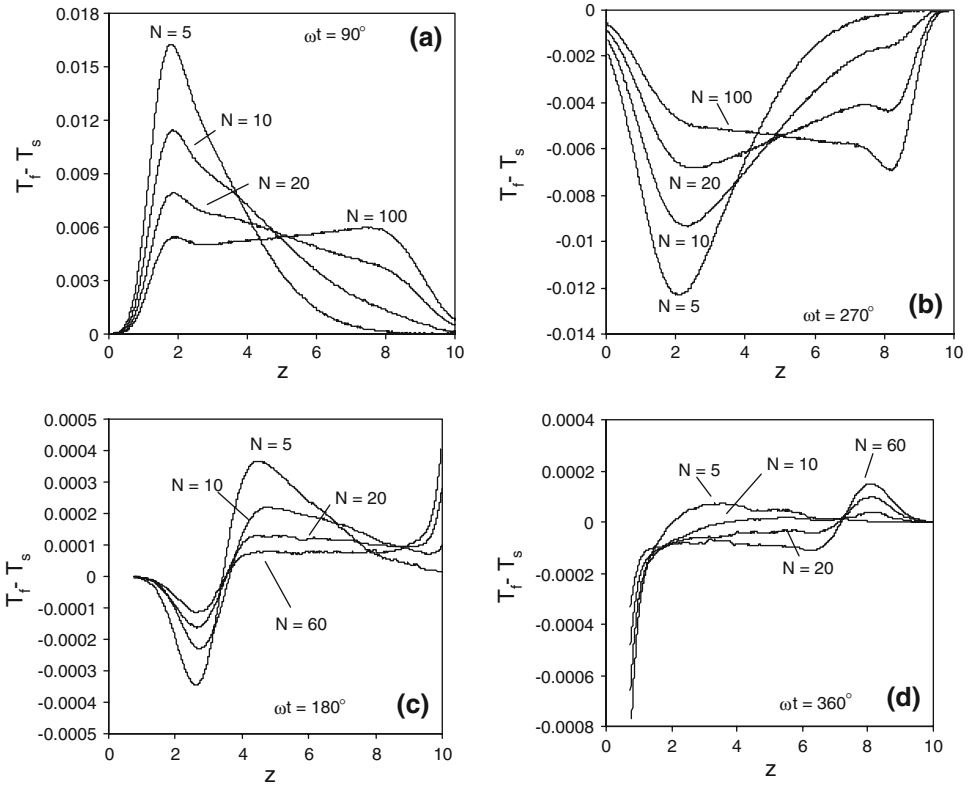


**Fig. 4** The variation of the temperature differential between the fluid and solid phases with distance for a glass-water bed. **a** Middle of hot phase, $\omega t = 90°$; **b** Middle of cold phase, $\omega t = 270°$; **c** end of the hot phase, $\omega t = 180°$; **d** end of the cold phase, $\omega t = 360°$. $Re = 100$, $L = 10$, $\omega = 1$

before steady state is reached. Figure 4a, b show the temperature differential at the middle of hot and cold phases, respectively. Figure 4c, d is a companion plot at the end of the hot and cold phases. Figure 4a looks similar to Fig. 3d where the variation of amplitude of temperature fluctuations in the bed is shown. The porous bed is divided into two parts about its midpoint where the signs of thermal non-equilibrium are opposite to each other. In the region closer to the inflow plane ($z = 0$), it is high but decreases with the number of cycles. It is a minimum at steady state. In the region closer to the outflow plane, its value is low during unsteady evolution. It increases with the number of cycles and becomes nearly a constant when steady state is reached. Close to the center of the bed ($z = L/2$), the temperature differential remains uniformly small during the transient evolution.

At the two ends of the bed, the fluctuations are unequal at the middle of the two phases ($\omega t = 90$ and 270°). At the hot end, $z = 0$, they fluctuate between zero and a negative value and at the cold end, $z = 10$, between a positive value and zero when steady state is reached.

Figures 4c, d show the variation of the temperature differential at the end of the two phases ($\omega t = 180$ and 360°). Fluctuations at these instants are uniformly small except for an increase at the two ends of the bed. The degree of non-equilibrium during the hot phase is higher when heat transfer is unsteady; correspondingly it is lower for the cold phase.

### 5.3 Energy storage

Thermal energy is stored in the bed during the hot phase, and retrieved during the cold phase by cold flow introduced at the right boundary. It is stored in the solid as well as the fluid phases of the bed, reaching a maximum level at steady state. Apart from the energy stored, some energy is lost through the cold end during the hot phase. Averaged over a half-cycle, its value for the present calculation is 2.1%. When the cold inflow leaves the bed at $z = 0$, the fluid temperature at the hot end is less than the ideal value of unity. The effectiveness of the bed has been calculated to be 98.3%. At cyclic steady state, the stored energy in the solid (glass) and fluid (water) phases has been computed to be 40.5 and 52.2% of the total supplied energy. The energy balance for the incoming and outgoing thermal energies is given by the factor $\psi$ in Eq. 19 and has been found to be 0.5%. This number can be taken as a measure of uncertainty in the numerical computation of effectiveness.

## 6 Parametric study

Effects arising from changes in bed parameters on temperature profiles and energy storage are discussed in the following sections.

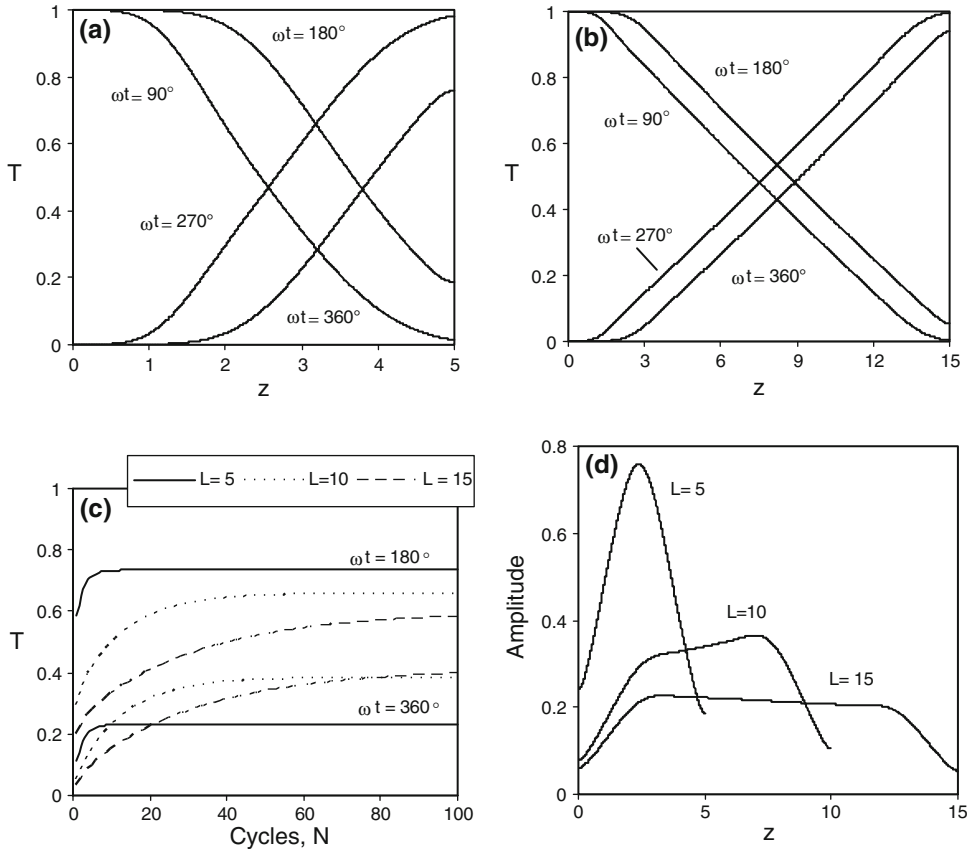


**Fig. 5** Effect of bed length on fluid temperature distribution in a glass water bed: **a** $L = 5$, **b** $L = 15$, **c** average temperature, **d** amplitude of temperature fluctuations. $Re = 100$, $\omega = 1$

### 6.1 Effect of bed length

The effect of length on thermal performance of the glass-water bed is shown in Fig. 5, with $L = 10$ being the reference configuration. Figure 5a and b show temperature profiles with respect to distance at steady state for bed lengths of $L = 5$ and 15, respectively. The average temperature calculated over the entire bed and distribution of temperature amplitude as a function of length are shown in Fig. 5c and d. A change in length has a definite effect on the average temperature of the bed during each of the hot and cold phases. A decrease in length results to lower storage space as compared to the reference. Subsequently one obtains a higher average temperature during the hot phase and a lower temperature during the cold phase. The temperature fluctuations and exit loss through the cold end during the hot phase are higher for $L = 5$ as compared to the reference. The exit losses increase with a reduction in length of the bed and hence lower the effectiveness to 94% as against 98.3% for the reference. In contrast, as the length of the bed is increased, the bed temperatures are lower during the hot phase and higher during the cold phase. For a lower bed length, the temperature amplitude peaks at the mid-plane (at $z = 2.5$ for $L = 5$) and falls rapidly with distance. For a long bed ($L = 15$), thermal fluctuations are of uniform amplitude. An increase in bed length results into lower exit losses but the storage capacity of the bed is not fully utilized.

Figure 5c shows the variation of average fluid temperature as a function of the number of cycles elapsed. At the end of the hot phase ($\omega t = 180°$), temperatures corresponding to $L = 5$ are the highest and those for $L = 15$ the lowest. At the end of the cold phase ($\omega t = 360°$), the profile for $L = 5$ has the lowest value and that for $L = 15$ the highest. These translate into low and high temperature fluctuations as shown in Fig. 5d. The number of cycles required to reach steady state depends on the length of the bed. The bed of length $L = 5$ reaches steady state quite early as compared to other beds. From Fig. 5c, the number of cycles required for attaining steady state is 18 ($L = 5$), 36 ($L = 10$) and 55 ($L = 15$), respectively. The near-linear dependence on length shows that energy transport along the length of the bed is advection-controlled.

### 6.2 Effect of frequency

The effect of frequency on temperature profiles is shown in Fig. 6. Since frequency is related to time period, a higher frequency indicates less time available for storage and retrieval of energy. On the other hand, with reduction in frequency, the supply of energy is higher, changes in temperature are higher and lead to higher amplitudes of

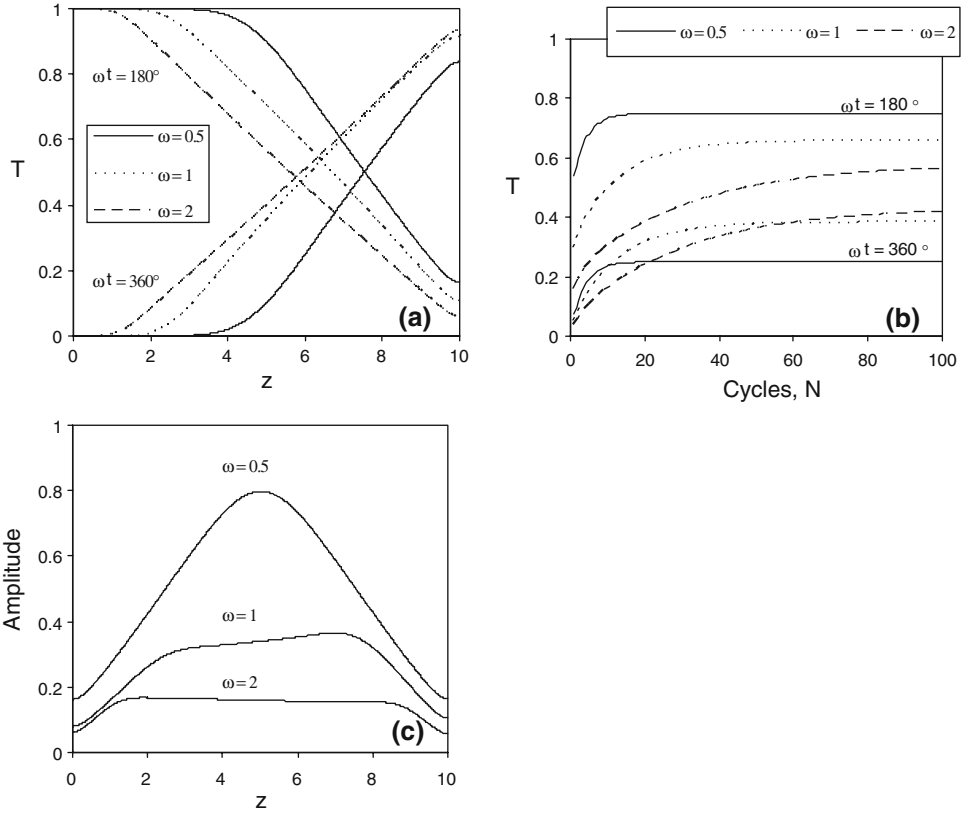


**Fig. 6** Effect of pulsing frequency on fluid temperature distribution in a glass-water bed: **a** temperature profiles, **b** length-averaged fluid temperature, **c** amplitude of temperature fluctuations. $Re = 100$, $L = 10$

temperature fluctuation. In the present discussion, Fig. 6, frequency has been changed from the reference value of unity to $\omega = 0.5$ and 2, while the bed length is 10 units and $Re = 100$.

At a frequency of $\omega = 0.5$, the storage of energy in the bed during the hot phase is larger, resulting in a higher temperature over the bed length. At the end of the hot phase, the profile corresponding to $\omega = 0.5$ has the highest temperature and the corresponding exit losses are also the highest. Temperatures are lower during the cold phase since a larger amount of energy is retrieved. The corresponding amplitude of temperature (defined here as the difference between the highest and the lowest) is the highest; this trend is shown in Fig. 6c. For $\omega = 0.5$, the peak value obtained at the center of the bed is very high at 0.80 but falls rapidly with distance on either side. For $\omega = 2$, the temperature build up is slower during the hot phase, and results in a lower temperature rise at the end of the hot phase. During the cold phase, the temperature drop is smaller than for $\omega = 1$. Hence, temperature fluctuations are smaller as shown in Fig. 6c. The fluctuations for $\omega = 2$ are the lowest for the three frequencies considered and are uniform throughout the bed. The exit losses corresponding to a frequency of $\omega = 2$ are also a minimum. The number of cycles required to reach steady state is the highest for $\omega = 2$ and the least for $\omega = 0.5$. This result derives from the increased dimensional time available at lower frequencies. Hence, in dimensional form, the time required to reach steady state depends mainly on the fluid speed but not the frequency of pulsation.

The effectiveness of energy storage is reported for each frequency. For $\omega = 0.5$, its value is 97.4%. For $\omega = 2$, the effectiveness is 98.3%. Since the time for which a hot phase lasts is higher at a lower frequency, the stored energy is greater. At a frequency greater than the reference, the stored energy is smaller. Effectiveness does not indicate the true amount of energy stored in the bed but is a measure of the recovery mechanism over a complete cycle. The energy input is, however, a function of frequency. For $\omega = 0.5$, the energy stored is 1.82 times that of the reference but for $\omega = 2$, it is lowered by a factor of 0.53. Hence decreasing frequency results in an increase in stored energy levels though exit losses are also marginally higher. Exit losses are greater by a factor of 2.25 with respect to the reference for $\omega = 0.5$; for $\omega = 2$, this factor is reduced to 0.37. The near-equal values of effectiveness shows that the fractions of incoming energy stored in the solid phase are quite close for the three frequencies.

### 6.3 Effect of particle size

The effect of change of particle size $d_p$ on temperature variation in the glass-water bed is shown in Fig. 7. Particle size slightly affects the porosity of the bed. The real effect

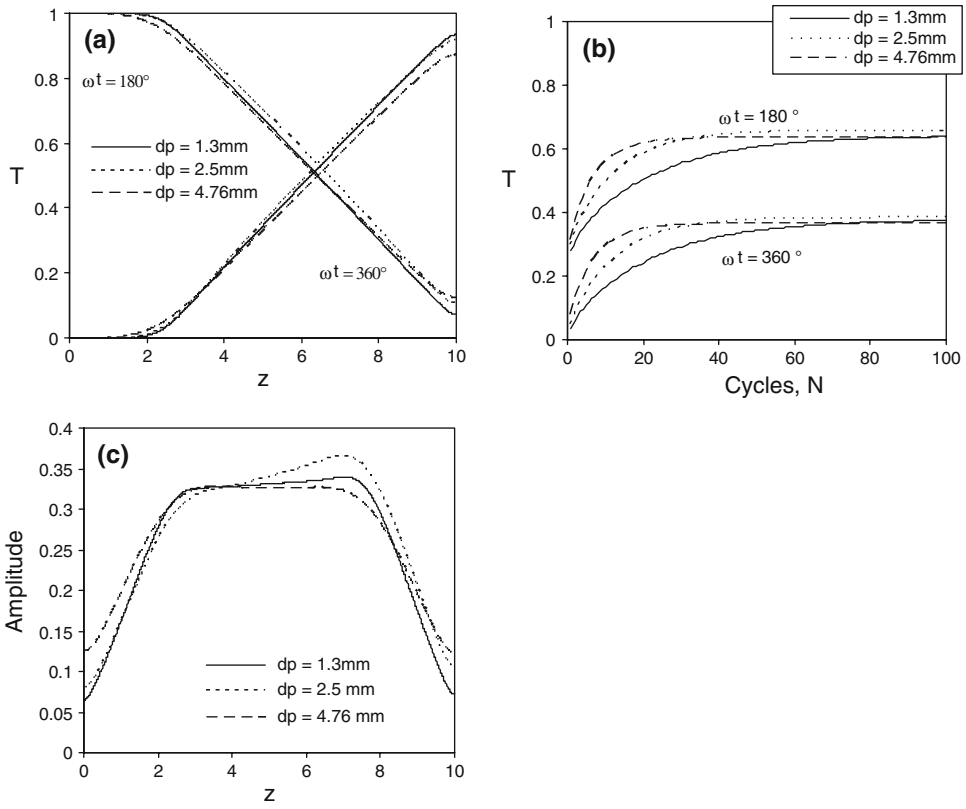


**Fig. 7** Effect of particle size in a glass-water bed. **a** Fluid temperature as a function of distance; **b** Unsteady average fluid temperature as a function of cycle number; **c** Amplitude of temperature fluctuations as a function of distance; $Re = 100$, $L = 10$, $\omega = 1$

is in terms of the interphase heat transfer area, given by Eq. 5. The surface area of the solid phase per unit volume of the bed increases with a reduction in $d_p$. Indirectly, particle size affects dispersion (Eqs. 3–6) and hence the spreading rate of thermal fronts in the porous medium. To examine these effects, the particle size has been changed from 2.5 mm for the reference bed to 1.3 and 4.76 mm during simulation. The corresponding values of porosity are 0.30 and 0.40, respectively.

Figure 7a shows that the steady-state fluid temperature variation in the bed is only a weak function of particle size. Figure 7b shows the average temperature in the glass-water bed as a function of number of cycles elapsed. During the unsteady period, the temperature corresponding to $d_p = 4.76$ mm is the highest during the hot phase. It is also highest during the cold phase. A higher particle size results in a lower interphase area and hence higher fluid temperature. At steady state, the differences in temperature are small. The improvement in the speed required to reach steady state can be partly related to increased dispersion at higher particle diameters.

The steady state variation of amplitude of temperature fluctuations with distance is shown in Fig. 7c for various particle diameters. These values are only marginally affected by the particle diameter. The temperature amplitudes are nearly uniform over the bed length but fall near the cold and the hot ends. The fluctuations near the ends are the highest for $d_p = 4.76$ mm. This trend can be explained as follows: Higher particle size has a lower storage space in the form of solid particles but more space for the stagnant fluid. For $d_p = 1.3$ mm, the energy in the solid phase is the highest but that in the fluid phase the lowest. The reverse happens for $d_p = 4.76$ mm. The energy stored in the solid phase is 107 and 93%, respectively of the reference case but that in the fluid phase is 78 and 106%. The corresponding values for exit losses are 1.1 and 3.4%, respectively. The overall energy storage levels are the lowest for $d_p = 1.3$ mm but the highest for $d_p = 4.76$ mm. The value of the energy balance factor $\psi$ for $d_p = 1.3$ and 4.76 mm were calculated, respectively as 0.1 and 0.05% during numerical simulation.

## 7 Effect of solid phase properties

In this section, the effect of change in thermal properties of the solid phase on the performance of the bed is discussed. For comparison, a steel water bed is considered. The values of thermal storage capacity ratio $\beta$ and thermal conductivity ratio $\lambda$ are changed from the reference values of 2.2 and 0.55 to 1.1 and 0.04, keeping the other parameters of the bed unchanged. The thermal conductivity ratio falls by a factor of two, but the main difference is in terms of the conductivity ratio, the thermal conductivity of steel being much greater than water.

### 7.1 Steel-water bed

Figure 8 compares fluid temperature profiles and several related quantities as obtained in glass-water and steel-water beds. Figure 8a shows the comparison of temperature–distance profiles at the end of the hot and cold phases. By the end of the hot phase, temperatures in the steel-water bed are lower than for glass-water bed. At the end of the cold phase, it has a higher temperature than that of the glass-water bed. The difference between the two profiles decreases at the hot and the cold ends. For example, during the hot phase, the maximum temperature at the cold end is 0.094 in a steel-water bed but its value is higher at 0.105 in glass-water bed. During the cold phase, the minimum temperatures at the hot end are equal for the two beds at 0.92. Figure 8b shows the comparison of midpoint fluid temperature with respect to number of cycles elapsed. The temperature at the end of the hot phase is higher in glass-water bed as compared to that of the steel-water bed but at the end of the cold phase, it is lower. Lower temperatures in water (during the hot phase) in the steel-water bed are explained by the higher thermal conductivity of steel that permits better thermal equalization in the solid phase.

The temperature fluctuations shown in Fig. 8c are lower for steel-water bed as compared to that for glass-water. The damping effect of temperature fluctuation in the steel-water bed is again related to the higher thermal conductivity of steel when compared to glass. The peak of temperature amplitude is towards the cold end at $z = 8$. This comparison is for insulated beds. A minor heat loss for steel-water has a stronger effect as compared to the glass-water bed. The authors in their earlier study [24] have discussed this aspect.

Figure 8d compares the degree of thermal non-equilibrium in the two beds at steady state as a function of distance from the hot end. It is plotted for the middle of the hot and the cold phases ($\omega t = 90°$ and $\omega t = 270°$, respectively). The trends are almost identical in the two beds with a peak value higher for the steel-water bed. At the middle of the hot phase, the peaks occur in both beds near $z = 2$, while at the middle of the cold phase, the peak is near $z = 8$. The extent of thermal non-equilibrium in the steel-water bed is higher as compared to that in a glass-water bed but the overall trends with distance are similar. The factor responsible for this result is the higher thermal capacity ($\rho C_p$) of steel when compared to glass. In numerical terms, however, the extent of thermal non-equilibrium is small, being of the order of 0.2–0.8%.

In the glass-water bed, the amount of energy leaving it during the hot phase is 2.1% whereas it is 2.6% in steel-water bed. The effectiveness of the steel water bed is 97.9% whereas it was 98.3% for glass-water. The fact that

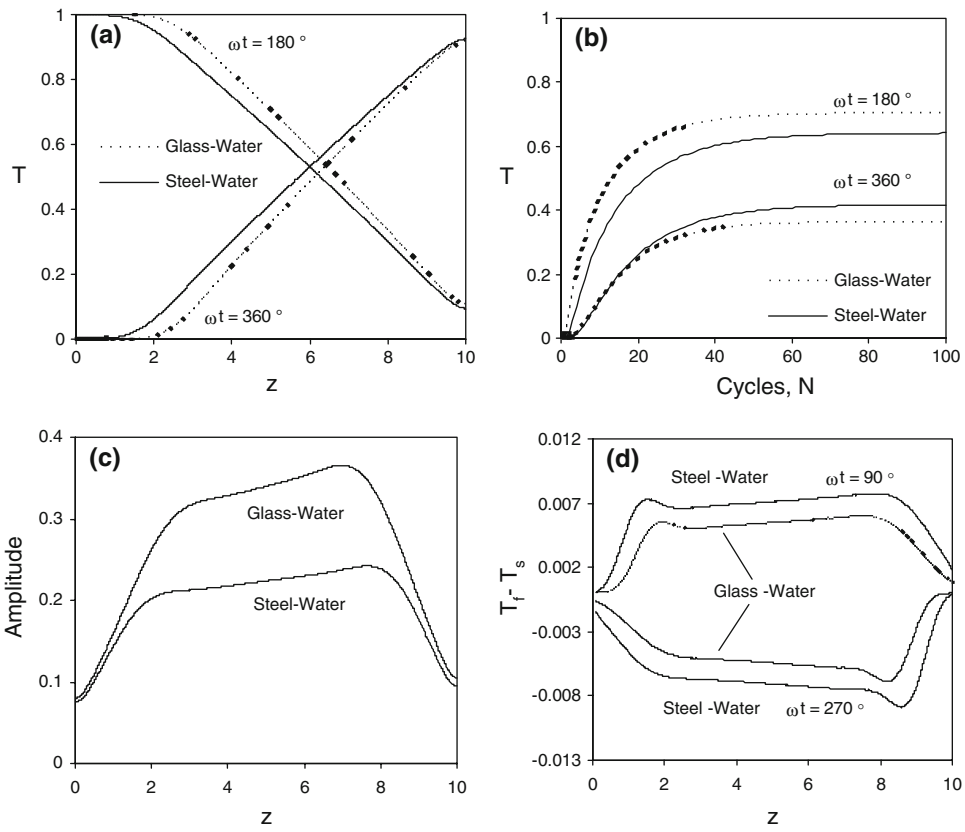


**Fig. 8** Comparison of thermal performance of glass and steel-water beds: **a** Fluid temperature as a function of distance, **b** Unsteady midpoint fluid temperature as a function of cycles elapsed, **c** amplitude of temperature fluctuations as a function of distance, **d** extent of thermal non-equilibrium as a function of distance. $Re = 100$, $L = 10$, $\omega = 1$

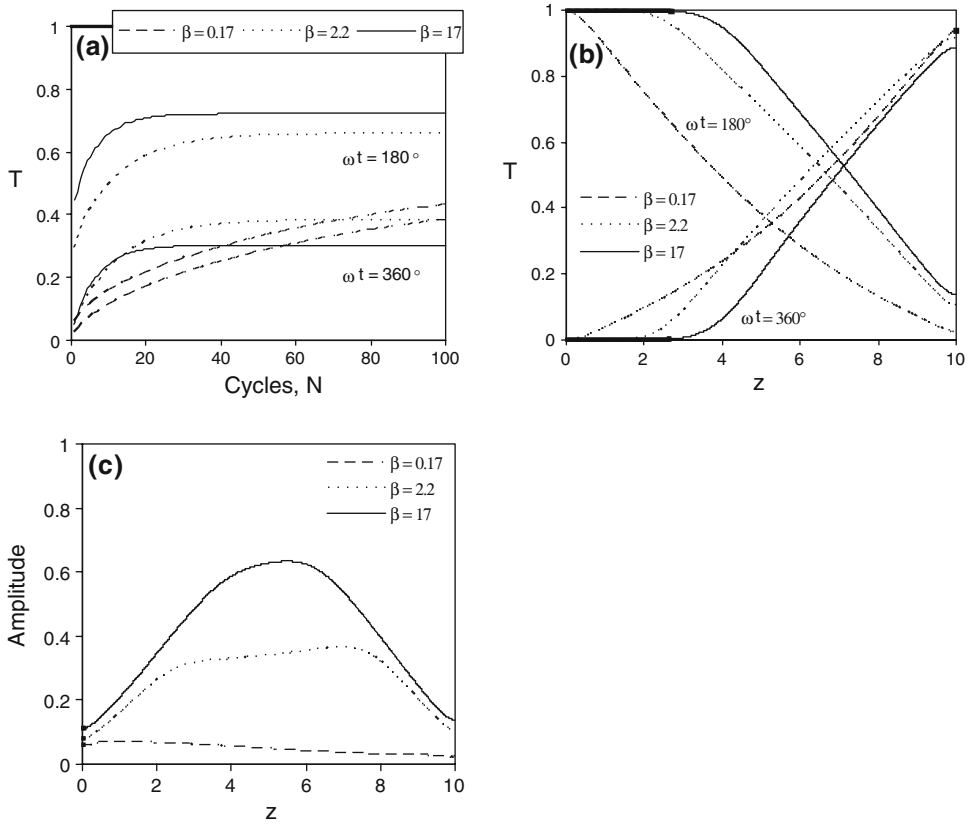


**Fig. 9** Effect of thermal capacity ratio: **a** unsteady midpoint fluid temperature as a function of cycles elapsed, **b** temperature profile as a function of distance, **c** amplitude of temperature fluctuations as a function of distance; $Re = 100$, $L = 10$, $\omega = 1$

steel has a higher storage capacity as compared to that of glass results into lower temperature fluctuations in the steel-water bed. The steel-water bed stores more energy in its solid phase than that in the glass-water bed. It has higher heat losses at the exit plane due to a higher thermal conductivity of steel when compared to glass.

### 7.2 Effect of thermal storage capacity ratio

In applications, it is expected that a significant variation will occur with respect to the thermal capacity ratio ($\beta$). Hence, a separate study with respect to this parameter has been carried out. The major property governing energy storage is the weighted ratio of solid and fluid phase thermal storage capacities given as $K$. However, in the present analysis, the equivalent property considered is $\beta$, the two are related to each other by $K = \frac{1-\varepsilon}{\varepsilon\beta}$. The value of $\beta$ is changed from its normal value of 2.2 in either directions, keeping the thermal conductivity ratio $\lambda$ a constant. Figure 9 shows the effect of change of properties on the average temperature in the bed. In Fig. 9a, mid-point temperature is plotted as a function of number of cycles elapsed at the end of the hot and cold phases. A decrease in the value of $\beta$ results in an increase in the storage capacity of the solid phase relative to that of the fluid phase, and the speed of response, namely time required to reach steady state becomes slower. Changing $\beta$ to 0.17, the temperature at the end of the hot phase is lower as compared to that of the reference and the rate of temperature build up is also quite slow. Its value at the end of the cold phase is marginally lower than that at the end of the hot phase. Overall, the temperature fluctuation is very small for $\beta = 0.17$ (Fig. 9c). On the other hand, an increase in $\beta$ to 17, results in an increase in storage capacity of the fluid phase, and the resulting temperature changes are large. At the end of the hot phase, the average temperature is higher and that at the end of the cold phase is very low with respect to the reference case. Hence, the amplitude of temperature fluctuations increases with an increase in the value of thermal capacity ratio $\beta$.

Figure 9b shows temperature profiles as a function of distance from the respective ends after cyclic steady state is reached. During the hot phase, the profile corresponding to $\beta = 0.17$ has the lowest temperature but during the cold phase the trend is reversed. The resulting amplitude of temperature fluctuations is shown in Fig. 9c. Its value for $\beta = 0.17$ is low but uniform throughout the bed and that for $\beta = 17$ is high at the midpoint ($z = L/2$) but falls on either side.

Figure 10 shows the extent of thermal non-equilibrium as a function of distance from the hot end for three different thermal capacity ratios. Figure 10a shows the thermal non-

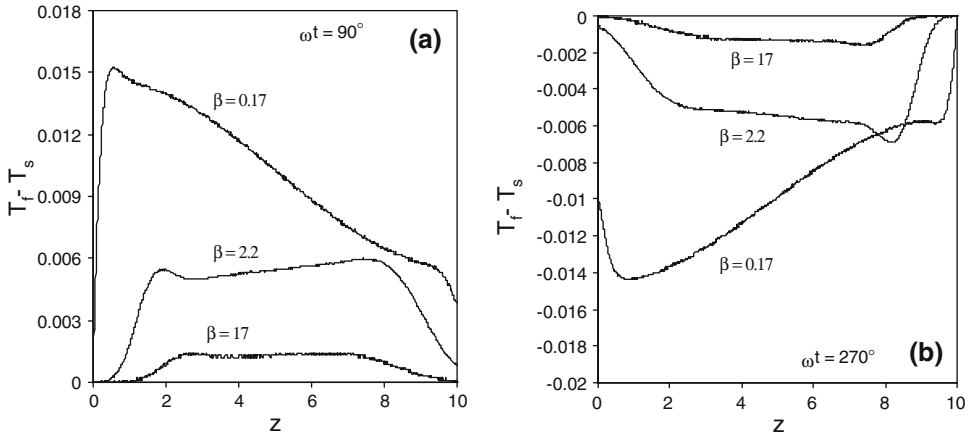


**Fig. 10** Effect of thermal capacity ratio: the variation of degree of thermal non-equilibrium is plotted as a function of distance along the bed. $Re = 100$, $L = 10$, $\omega = 1$

equilibrium at the middle of the hot phase ($\omega t = 90°$) while Fig. 10b is at the middle of the cold phase ($\omega t = 270°$). Thermal non-equilibrium, measured as the difference between the fluid and solid temperatures is numerically the highest in both cases for $\beta = 0.17$. However, these value for $\beta = 17$ are small. Hence, thermal non-equilibrium is higher when the solid phase has a larger storage capacity than the fluid phase. A change in thermal properties affects the relative storage capacities of the fluid and solid phases. For a glass-water bed, the solid phase stores around 43% of the total energy and the rest is in the fluid phase. For $\beta = 0.17$, the share of the solid phase rises to 91% but for $\beta = 17$, it is only 9%. Hence, it is the question of storing the energy in a particular form. It is preferable to store energy in the solid phase rather than the fluid phase because it is stagnant. Figure 9 shows that temperature fluctuations are higher for $\beta = 17$ and results in a higher hot phase temperatures at the end of the half-cycle. The exit losses are thus higher for $\beta = 17$ as the temperature levels are higher. It can also lead to severe heat loss to the ambient when compared to lower values of $\beta$. From these considerations, energy storage in porous beds with a higher value of $\beta$ is a better alternative.

The other property of interest is the thermal conductivity ratio $\lambda$. Simulation showed that a change in its value did not affect very much the temperature profiles and they remained nearly unchanged. A low value of $\lambda$ coupled with higher thermal losses to the ambient significantly diminished effectiveness of the energy storage system.

Figure 11 shows the energy stored as a function of the thermal capacity ratio $\beta$. Figure 11a shows the total energy stored in various porous beds as fraction of that stored in the glass-water bed for which $\beta = 2.2$. A bed with $\beta = 1.1$ stores 4% more energy though the temperature levels are less. A bed with $\beta = 0.17$ stores 10% more energy as compared to that of the glass-water bed but a bed with $\beta = 17$ stores only 95% of the reference. A higher storage compared to the glass-water bed shows that the exit losses are correspondingly lower. Hence, a marginal change in the total stored energy occurs with a change in the value of $\beta$. Figure 11b shows the fraction of energy stored in the solid and the fluid phases. A glass-water bed stores 43% of the total energy in the solid phase whereas the corresponding value for steel-water is 61%. The storage in the solid phase for a porous bed with $\beta = 0.17$ is as high as 91% but for $\beta = 17$, it is only 9%. It can be concluded that the role of

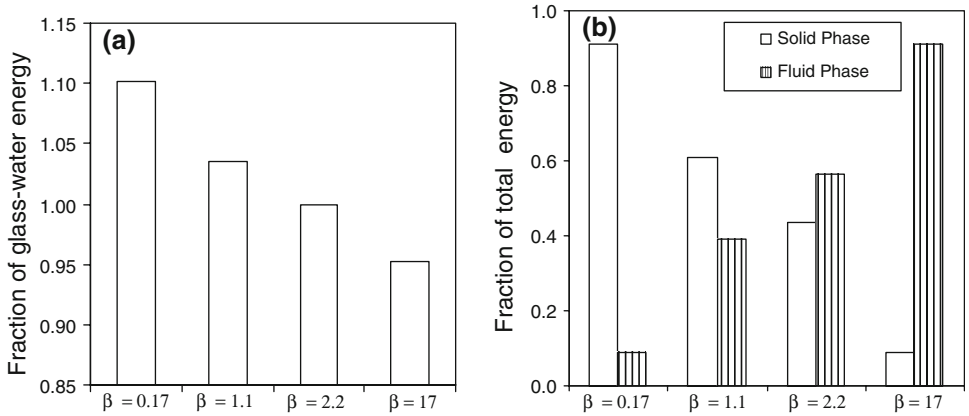


**Fig. 11** Energy storage in porous medium: **a** Fraction of glass-water bed energy, **b** storage in the solid and the fluid phases. $Re = 100$, $L = 10$, $\omega = 1$

thermal capacity ratio is important for an energy storage system and thermal conductivity is of less importance.

## 8 Conclusions

Numerical simulation of oscillatory flow in a porous bed using the 2-equation model is reported. Two combinations, namely, glass- and steel-water have been studied. Quantities such as temperature profiles, temperature amplitudes, degree of thermal non-equilibrium, and effectiveness of energy storage are presented. Their dependence on the bed length, frequency, particle size and the solid phase properties has been examined. Conclusions arrived in the present work are summarized below

1. Temperature profiles change with the time instant considered within a cycle. Accordingly, temperature amplitudes and degree of thermal non-equilibrium depend on the phase under question.
2. For the nominal set of parameters studied, temperature profiles were close to linear over the length of the porous region, temperature amplitude nearly a constant, with negligible thermal non-equilibrium in a glass-water bed. Though the effectiveness of the porous region remained high (>95%), the energy stored in the bed was seen to be a function of length, frequency, and property ratios.
3. *Effect of length*: A shorter length creates greater temperature pulsations while a longer bed reveals smaller temperature amplitudes. Exit losses increase when the bed length is decreased. Time required to reach steady state increases linearly with the bed length.
4. *Effect of frequency*: A lower frequency results in greater temperature uniformity at the end of the half-cycle and hence higher stored energy and temperature amplitudes. The exit losses are also higher. An opposite trend is seen at higher frequencies. In addition, cycles required to reach steady state is higher at higher frequencies.
5. *Effect of thermal capacity ratio*: A lower thermal capacity ratio provides more energy storage in the solid phase in comparison to the fluid. Total energy stored in the porous medium increases. Temperature fluctuations decrease with decreasing thermal capacity ratio.
6. *Effect of thermal conductivity ratio*: Thermal conductivity ratio does not significantly affect the performance of the porous region. It is a relevant parameter when losses to the ambient are considered, with a higher value preferred.

## References


1. Walker G (1983) Cryocoolers, Part 1 and 2, international cryogenics monographs series. Plenum Press, New York
2. Brisson JG, Swift GW (1994) Measurements and modeling of recuperator for superfluid stirling refrigerator. Cryogenics 34:971–982
3. Kuzay TM, Collins JT, Khounsary AM, Morales G (1991) Enhanced heat transfer with metal wool filled tubes. In: Proceedings of the ASME/JSME thermal engineering conference, pp 145–151
4. Amiri A, Vafai K (1994) Analysis of dispersion effects and non-thermal equilibrium, non-Darcian, variable porosity, incompressible flow through porous media. Int J Heat Mass Transfer 37:939–954
5. Kuznetsov AV (1994) An investigation of a wave of temperature difference between solid and fluid phases in a porous packed bed. Int J Heat Mass Transfer 37:3030–3033
6. Koh JCY, Colony R (1974) Analysis of cooling effectiveness for porous material in a coolant passage. ASME J Heat Transfer 96:324–330
7. Koh JCY, Stevens RL (1975) Enhancement of cooling effectiveness by porous materials in coolant passage. ASME J Heat Transfer 97:309–311
8. Bejan A (1978) Two thermodynamic optima in the design of sensible heat units for energy storage. ASME J Heat Transfer 100:708–712
9. Beasley DE, Clark JA (1984) Transient response of a packed bed for thermal energy storage. Int J Heat Mass Transfer 27:1659–1669
10. Muralidhar K, Suzuki K (1997) Regenerator models for Stirling cycles. Thermal Sci Eng 5:31–40
11. Chikh S, Boumedien A, Bouhadef K, Lauriat G (1998) Analysis of fluid and heat transfer in a channel with intermittent heated porous blocks. Heat Mass Transfer 33:405–413
12. Paek JW, Kang BH, Hyun JM (1999) Transient cool-down of a porous medium in pulsating flow. Int J Heat Mass Transfer 42:3523–3527
13. Muralidhar K, Suzuki K (2001) Analysis of flow and heat transfer in a regenerator mesh using a non-Darcy thermally non-equilibrium model. Int J Heat Mass Transfer 44:2493–2504
14. Dincer I, Rosen MA (2001) Energetic, environmental and economic aspects of thermal energy storage systems for cooling capacity. App Thermal Eng 21:1105–1117
15. Fu HL, Leong KC, Huang XY, Liu CY (2001) An experimental study of heat transfer of a porous channel subjected to oscillating flow. ASME J Heat Transfer 123:162–170
16. Leong KC, Jin LW (2005) An experimental study of heat transfer in oscillating flow through a channel filled with an aluminum foam. Int J Heat Mass Transfer 48(2):243–253
17. Byun SY, Ro TS, Shin JY, Son YS, Lee DY (2006) Transient thermal behavior of porous media under oscillating flow condition. Int J Heat Mass Transfer 27:1659–1669
18. Cheralathan M, Velraj R, Renganarayanan S (2007) Effect of porosity and the inlet heat transfer fluid temperature variation on the performance of cool thermal energy storage system. Heat Mass Transfer 43:833–842
19. Kaviany M (1991) Principles of heat transfer in porous media. Springer, Heidelberg
20. Nakayama A, Kuwahara F, Sugiyama M (2001) A two energy equation model for conduction and convection in porous media. Int J Heat Mass Transfer 44:4375–4379
21. Wakao N, Kaguei S (1982) Heat and mass transfer in packed beds. Gordon and Breach Science Publishers, New York

22. Wakao N, Kaguei S, Funazkri T (1979) Effect of fluid dispersion coefficient on particle-to-fluid heat transfer coefficients in packed beds. Chem Eng Sci 34:325–336
23. Leonard BP (1979) A stable and accurate convective modeling procedure based on quadratic upstream interpolation. Comp Methods Appl Mech Eng 19:59–98
24. Singh Chanpreet, Tathgir RG, Muralidhar K (2006) Experimental validation of heat transfer models for flow through a porous medium. Heat Mass Transfer 43:55–72